

## Nervous System Involvement in COVID-19: Results from a Retrospective Consecutive Neuroimaging Cohort

Stefanos Klironomos, MD, PhD<sup>1,2\*</sup>; Antonios Tzortzakakis, MD<sup>1,3\*</sup>; Annika Kits, MD<sup>1,2</sup>; Claes Öhberg, MD<sup>1,2</sup>; Evangelia Kollia, MD<sup>11</sup>; Amir Ahoromazdae, MD<sup>4</sup>; Håkan Almqvist, MD<sup>1,2</sup>; Åsa Aspelin, MD<sup>1,2</sup>; Heather Martin, MD, FRCPC<sup>1</sup>; Russell Ouellette, BSc<sup>1,2</sup>; Jonathan Al-Saadi, BSc<sup>2</sup>; Mikael Hasselberg, MSc<sup>1,2</sup>; Mansour Haghgou, MSc<sup>1</sup>; Mitra Pedersen, BSc<sup>1</sup>; Sven Petersson, MSc, PhD<sup>3,5</sup>; Johannes Finnsson, MD, PhD<sup>1,2</sup>; Johan Lundberg, MD, PhD<sup>1,2</sup>; Anna Falk Delgado, MD, PhD<sup>1,2</sup>; Tobias Granberg, MD, PhD<sup>1,2</sup>

\*S.K. and A.T. contributed equally to this work.

### Affiliations

1. Department of Neuroradiology, Karolinska University Hospital, Stockholm, Sweden.
2. Department of Clinical Neuroscience, Karolinska Institutet, Stockholm, Sweden.
3. Department of Department of Clinical Science, Intervention and Technology, Karolinska Institutet, Stockholm, Sweden.
4. Department of Neurology, Karolinska University Hospital, Stockholm, Sweden.
5. Department of Medical Radiation Physics and Nuclear Medicine, Karolinska University Hospital, Stockholm, Sweden.

### Corresponding author

Tobias Granberg

Department of Neuroradiology, O42  
Karolinska University Hospital

141 86, Stockholm, Sweden  
tobias.granberg@ki.se

### Contributions

AT, SK and TG initiated the study. AK, CÖ and TG designed the standardized clinical MRI protocol; MH, MH, MP, SP and TG implemented it. AT, SK, AK, CÖ, EK, HA, ÅA, HM, JF, JL, AFD and TG performed systematic re-evaluations of all imaging. AFD post-processed MRI perfusion data. AK, JL and AFD interpreted MRI perfusion data. AT, SK, CÖ, EK, AA and JA evaluated clinical data. SK, RO, JA and TG organized data. AT, SK, RAO and TG wrote the first draft and all authors revised the manuscript critically. All authors approved the final version of the manuscript.

**Article Type:** Original Research Article

### Abbreviations

95%-CI = 95% confidence interval, COVID-19 = coronavirus disease 2019, FLAIR = fluid-attenuated inversion recovery, PCR = polymerase-chain-reaction, rCBF = relative cerebral blood flow, SARS-CoV-2 = severe acute respiratory syndrome coronavirus 2, SWI = susceptibility-weighted imaging.

### Key Results

- In patients with COVID-19 who required neuroimaging, intra-axial susceptibility abnormalities were the most common finding (29/39, 74%, of patients with brain MRI), often with an ovoid shape suggestive of microvascular pathology, and with a predilection to corpus callosum (23/39, 59%).
- A predilection of susceptibility abnormalities for juxtacortical white matter was seen in 14/39 (36%) patients with COVID-19, similar to patients with other critical illnesses.

### **Summary**

In hospitalized adults with COVID-19 undergoing neuroimaging, vascular and inflammatory changes are common, with frequent non-spherical susceptibility abnormalities on MRI suggestive of cerebral microvascular involvement.

## Abstract

**Background:** Neurological complications in coronavirus disease 2019 (COVID-19) have been described, but the understanding of their pathophysiology and neuroanatomical correlates remains limited.

**Purpose:** To report on the frequency and type of neuroradiological findings in COVID-19.

**Materials and Methods:** In this retrospective study, all consecutive adult hospitalized patients with PCR-positivity for SARS-CoV-2, undergoing neuroimaging at Karolinska University Hospital between March 2 and May 24, 2020, were included. All examinations were systematically re-evaluated by 12 readers. Summary descriptive statistics were calculated.

**Results:** 185 patients with COVID-19 ( $62 \pm 14$  years, 138 men) underwent neuroimaging. In total, 222 brain CT, 47 brain MRI and 7 spinal MRI scans were performed. Intra-axial susceptibility abnormalities were the most common finding (29 of 39 [74%, 95%-CI 58–87%]) in patients with brain MRI, often with an ovoid shape suggestive of microvascular pathology, and with a predilection to corpus callosum (23 of 39, [59%, 95%-CI 42–74%]) and juxtacortical areas (14 of 39, [36%, 95% CI 21-53%]). Ischemic and macrohemorrhagic manifestations were also seen, but vascular imaging did not reveal overt abnormalities. Dynamic susceptibility contrast perfusion MRI in 19 patients did not reveal consistent asymmetries between hemispheres or regions. Many patients (18 of 41 [44%, 95%-CI 28–60%]) had leukoencephalopathy and one patient had a cytotoxic lesion of the corpus callosum. Other findings included olfactory bulb signal abnormalities (7 of 37, 19%), prominent optic nerve subarachnoid spaces (20 of 36, 56%), and enhancement of the parenchyma (3 of 20, 15%), leptomeninges (3 of 20, 15%), cranial nerves (2 of 20, 10%), and spinal nerves (2 of 4, 50%). At MRI follow-up, regression of leukoencephalopathy and progressive leptomeningeal enhancement was observed in one patient respectively, suggestive of dynamic processes.

**Conclusion:** Patients with COVID-19 had a wide spectrum of vascular and inflammatory involvement of both the central and peripheral nervous system.

## **Introduction**

Neurological symptoms in coronavirus disease 2019 (COVID-19) are increasingly reported. It remains debated to what extent these symptoms are manifestations of potential neurovirulence, secondary effects, general critical illness, or iatrogenic from complex symptom management (1,2). However, the incomplete understanding of their pathophysiological basis impedes the development of effective treatment strategies and portends long-standing effects on public health.

Wuhan had early reports of acute cerebrovascular lesions and impaired consciousness (3). These findings were later confirmed in other studies reporting macrovascular events (4), even in young patients (5), despite reductions in stroke imaging during the pandemic (6). Other early neuroimaging case reports in COVID-19 showed acute hemorrhagic necrotizing encephalopathy (7), and hippocampal signal abnormalities (8). A later detailed case report demonstrated leukoencephalopathy and susceptibility-weighted imaging (SWI) abnormalities in white matter and posterior hyperperfusion (9).

To date, large neuroimaging studies on COVID-19 are lacking, with most studies focusing on a smaller number of patients in the intensive care unit. A letter on neurological features in intensive care patients reported brain MRI findings in 13 patients, including 3 ischemic strokes, leptomeningeal enhancement in 8 patients, and frontotemporal hypoperfusion in all 11 patients who underwent perfusion imaging. (10). Some of these imaging findings have since been debated (11). In another retrospective intensive care study, 12 of 27 (44%) patients with neurological symptoms had brain MRI findings (12). Also, in hospitalized patients, 51 of 108 (47%) examined patients had neuroimaging abnormalities, most frequently infarcts and hemorrhages but also less commonly cerebral venous thrombosis, encephalopathy, posterior reversible encephalopathy syndrome, Guillain-Barré syndrome, and Miller-Fisher syndrome (13).

In a recent retrospective multicenter study, 37 patients with severe COVID-19 were consecutively sampled and underwent brain MRI with pathology. The results showed frequent signal changes in the mesial temporal lobe, variable contrast-enhancement of multifocal white matter hyperintensities, and SWI-abnormalities (14).

The purpose of this study was to report the frequency and type of neuroradiological findings in patients with COVID-19 based on all consecutive adult hospitalized patients imaged at our institution.

## **Materials and Methods**

### **Ethical considerations**

This retrospective study was approved by the Swedish Ethical Review Authority. Informed consent was waived due to the retrospective nature of the study and to avoid bias in participant inclusion, especially since many patients had impaired consciousness/cognition, were critically ill or deceased.

### **Study participants**

Included in this study were all consecutive adult ( $\geq 18$  years of age) hospitalized patients with positive reverse transcription-polymerase chain reaction (PCR) for SARS-CoV-2 that

underwent neuroimaging at Karolinska University Hospital in Stockholm, Sweden at two geographical sites between March 2 (first patient admitted) and May 24, 2020 (study conclusion). No exclusion criteria were applied in order to avoid biases in the reporting.

### **Imaging**

All imaging was performed according to clinical routine. Scanner allocation was based on the clinical and logistical needs. Iodine-based and gadolinium-based contrast agents were used cautiously as per standard of care due to the high frequency of renal failure and the need for dialysis in the patient group.

### **CT**

Brain CT was performed on the following scanner models: Canon Aquilion ONE Genesis (Canon Medical Systems, Otawara, Japan), GE Discovery CT750 HD and Revolution CT (GE Healthcare, Milwaukee, WI), Philips IQon Spectral CT (Philips Healthcare, Best, Netherlands) and Siemens SOMATOM Definition Flash (Siemens Healthineers, Erlangen, Germany). Scanning was performed with/without contrast agent in standard doses. Sub-millimeter spatial resolution images were acquired and reconstructed in three planes with 5-millimeter slice thickness.

### **MRI**

All MRI was performed on the following scanner models using standard clinical coils: GE Optima MR 450w GEM 1.5 T (GE Healthcare, Milwaukee, WI), Philips Ingenia 1.5 T (Philips Healthcare, Best, Netherlands), Siemens MAGNETOM Aera 1.5 T, Prisma<sup>fit</sup> 3.0 T, Skyra 3.0 T, Vida 3.0 T (Siemens Healthineers, Erlangen, Germany). Based on preliminary brain MRI findings on neurologic features in severe SARS-CoV-2 infection (10), we decided to implement a detailed standardized protocol for brain MRI in clinical practice, as detailed in Table 1. The technical MRI parameters are detailed in Table E1. When available, previous brain MRIs were also assessed.

### **Visual assessments**

All imaging was simultaneously and independently re-evaluated in a structured manner by 12 readers (author initials, clinical title, years of clinical experience in radiology): AT, neuroradiologist, 14; SK, neurologist, fellow in neuroradiology, 4; AK, neuroradiologist, 15; CÖ, neuroradiologist, 9; EK, fellow in neuroradiology, 14; HA, neuroradiologist, 22; ÅA, neuroradiologist, 9; HM, neuroradiologist, 20; JF, neuroradiologist, 10; JL, resident in radiology, 5; AFD, neuroradiologist, 10; TG, fellow in neuroradiology, 6. Some readers (AT, SK, CÖ, EK, JL, TG) were, in parallel, asked to systematically report on specific findings across all scans, to ensure homogenous evaluations across the sample. Meanwhile, some readers were asked to review a broad spectrum of pathology in a subset of CTs (HA, HM, JF), the complete sample of brain MRIs (AK, AFD) or spinal MRIs (SK, ÅA) to ensure that the whole perspective of findings was considered per patient. The initial ratings were performed blinded to the clinical data. All imaging aspects were reviewed by at least one board-certified neuroradiologist and disagreements in findings were resolved by consensus immediately after the all individual ratings had been performed.

We systematically evaluated findings previously reported in COVID-19 (see detailed references in the Introduction) or known from other human coronavirus infections (1) and findings encountered in other diseases and critical illness. When encountering findings in the

sample not previously reported in the literature, we reevaluated all scans based on the new aspect. Due to the lack of validated rating scales for COVID-19, we applied the Microbleed Anatomical Rating Scale (MARS) to quantify the burden of susceptibility abnormalities (15). As described by Chung et al, the 3D T<sub>2</sub>-FLAIR signal of the olfactory bulb was visually assessed (SK, AK, AFD); higher signal intensity than adjacent normal-appearing grey matter was considered abnormal (16). The presence of contrast-enhancement was assessed on 3D T<sub>1</sub>-weighted MRI.

### Perfusion analysis

Brain perfusion MRI was performed using dynamic susceptibility contrast (DSC) according to clinical routine (gadoteric acid; GE Healthcare, Milwaukee, WI; 0.1 mmol/kg). MRI perfusion images were post-processed in Philips IntelliSpace Portal version 10.1 (Philips Healthcare, Best, Netherlands) using the MRI Neuro Perfusion package and manual arterial input function (AFD). Perfusion MRI was, first, independently assessed by two neuroradiologists (AK, AFD) blinded to the clinical data and, immediately afterwards, disagreements were resolved by consensus. To objectively assess the findings, regions of interest were placed in grey and white matter supratentorial regions (AFD), exemplified in Figure E1. Relative cerebral blood flow (rCBF) was normalized against cerebellar blood flow to yield an rCBF ratio. Arterial spin labeling results are not presented due to the uncertainty in the interpretation of the findings when dynamic susceptibility contrast perfusion results were not overtly pathological.

### Statistical analysis

Descriptive statistics were obtained using R version 4.0.1 for Linux (R Core Team, Vienna, Austria).

## Results

### Patient demographics

Among 2611 patients with COVID-19, 185 (185/2611, 7.1%, 95% confidence interval [95%-CI] 6.1–8.1%; 62±14 years, 138 men) underwent neuroimaging based on clinical indication. A flow chart of the study is presented in Figure 1. The demographics of the study participants are summarized in Table 2.

### Frequency of imaging and findings

A total of 174 patients (174/2611, 6.6%, 95%-CI 5.7–7.7%) had 222 brain CT scans (median 1, range 1–4 scans). Brain MRI was performed in 43 patients (43/2611, 1.6%, 95%-CI 1.2–2.2%) with 47 brain MRI scans, of which 22 were contrast-enhanced; 4 patients had a follow-up MRI (median follow-up time 12, range 6–24 days). Seven patients underwent a spinal MRI (2 whole-spine, 2 cervical, 1 thoracic-lumbar, 2 lumbar) of which 4 were contrast-enhanced. The median time from symptom onset to scan was 21 days for CT and 34 days for MRI. The frequency of findings is summarized in Tables 3 and 4. All reported percentages refer to the number of patients with appropriate imaging to assess the pathology in question.

In asymptomatic/mildly symptomatic patients with incidental PCR-positivity, 43 brain CT scans (43/185 CT, 23%, 95%-CI 17–30%) and 2 brain MRI scans (2/47, 4.3%, 95%-CI 0.5–15%) were performed on indications unrelated to COVID-19. Head trauma was a common indication for CT. The most common indication for MRI was unexplained, prolonged consciousness impairment after extubation.

### **Macrovascular pathology**

Fifteen patients (15/174, 8.6%, 95%-CI 4.9–14%) had acute ischemic infarcts on CT, two of which showed hemorrhagic transformation (Figure 2 A-D). Eleven patients (11/174, 6.3%, 95%-CI 3.2–11%) had non-traumatic intraparenchymal hematomas on CT. One patient had an acute subdural hematoma related to a posterior cerebral hemorrhagic infarct (Figure 2 C-D). Two patients had intraparenchymal hematomas (1 frontal, 1 cerebellar) on MRI. Six patients had thin circumferential contrast enhancement (distal ICA, distal basilar, P1, M1-2 and A1 segments) on vessel wall (“black blood”) imaging.

### **Diffusion abnormalities**

Five patients presented with acute cortical infarcts (5/41, 12%, 95%-CI 4.1–26%) and five with acute lacunar small (<1.5 cm) infarcts (5/41, 12%, 95%-CI 4.1–26%) on brain MRI, (Figure 2 E-H). One patient presented with a cytotoxic lesion of the corpus callosum (Figure 2 J-L). Reduced diffusion with mild enhancement in the globus pallidus bilaterally was seen in 1 patient.

### **Susceptibility-weighted imaging abnormalities**

The most frequent MRI finding, seen in 29/39 (74%, 95%-CI 58–87%) patients, was SWI abnormalities of variable number and extent (Figure 3), often with ovoid or tubular appearance (Figure E2). There was a predilection to the splenium, the juxtacortical U-fibers and the main white matter tracts. SWI abnormalities were detected in the corpus callosum in 23/39 (59%, 95%-CI 42–74%) patients. Some patients with a high number of SWI abnormalities had focal reduced diffusion and/or confluent T<sub>2</sub>/FLAIR hyperintensities in the most affected areas and other brain areas. No difference in the intraparenchymal SWI abnormalities was seen across time in the patients who had follow-up MRI with SWI (N=3). Another common finding on SWI was the presence of small subarachnoid foci (9/39, 23%, 95%-CI 11–39%) including intraventricular blood (6/39, 15%, 95%-CI 5.9–31%) and cortical superficial siderosis (3/39, 7.7%, 95%-CI 1.6–21%). The median microbleed anatomical rating scale (MARS) score was 6.5 (range 0–26).

### **White matter changes**

White matter changes were common (23/41, 56%, 95%-CI 40–72%). Eighteen patients (18/41, 44%, 95%-CI 28–60%) had confluent, symmetric, periventricular lesions. Eleven patients (11/41, 27%, 95%-CI 14–43%) had involvement of the corpus callosum. One patient with diffuse symmetric leukoencephalopathy showed partial resolution with clinical improvement at follow-up (Figure 4). Ten patients (10/41, 24%, 95%-CI 12–40%) exhibited juxtacortical white matter changes and seven patients (7/41 17%, 95%-CI 7.2–32%) had white matter changes in the middle cerebellar peduncles.

One patient had bilateral symmetric white matter changes with reduced diffusion in occipital and frontal areas. These findings could represent diffuse leukoencephalopathy possibly related to hypoxemia as previously suggested in (17), or posterior reversible encephalopathy syndrome as previously reported in COVID-19 (13). Toxic/metabolic encephalopathy or encephalitis were considered as alternative diagnoses. Subtle regression of the white matter changes was seen on a follow-up MRI scan in one of the patients (Figure E3), who later succumbed to cardiorespiratory complications.

### **Contrast enhancement**

Intraparenchymal enhancement was detected in 3 patients (3/20, 15%, 95%-CI 3.2–38%) with subacute cortical infarction, adjacent to a subacute intracerebral hematoma and in one patient bilaterally in the globus pallidus. Three patients (3/20, 15%, 95%-CI 3.2–38%) had subtle leptomeningeal enhancement, most visible on post-contrast T<sub>2</sub>-FLAIR; One patient had a follow-up MRI where progression of leptomeningeal enhancement was demonstrated (Figure 5), although the patient improved clinically. Two patients exhibited cranial nerve enhancement; one bilaterally in the facial nerves (Figure 6 A-B), presenting with facial diplegia; the other in the right vestibular nerve (Figure 6 C-D), presenting with vestibular neuritis. Two patients exhibited enhancement along the cauda equina nerve roots, both presenting with acute demyelinating inflammatory polyneuropathy (Figure 6 E-F).

### **Olfactory bulbs and tracts**

Increased signal on T<sub>2</sub>-weighted FLAIR sequences in the olfactory bulbs/tracts was seen in 7/37 (19%, 95%-CI 8.0–35%) patients (Figure E4); in two, there was also subtle contrast enhancement.

### **Optic nerves**

Prominent subarachnoid spaces around the optic nerves were noted in 20 patients (20/36, 56%, 95%-CI 38–72%) on T<sub>2</sub>-weighted MRI sequences.

### **Perfusion findings**

Perfusion was assessed in 19 patients. rCBF ratios were mostly symmetric between white and grey matter regions respectively (Figure E5). rCBF ratios were similar across patients, with a white matter rCBF ratio of  $0.63 \pm 0.25$  and a grey matter rCBF ratio of  $1.05 \pm 0.36$  (mean  $\pm$  standard deviation).

### **Previous brain MRI findings**

Previous brain MRI was available in 9/43 (21%, 95%-CI 10–36%) patients (time difference:  $7.5 \pm 7.9$ , range: 1.2–25 years). Pre-existing conditions included macrovascular events or degenerative/microvascular changes and multiple sclerosis.

### **Discussion**

We report on neuroradiological observations in 2611 consecutive hospitalized adults hospitalized with COVID-19 where 7.1% (95%-CI 6.1–8.1%) underwent neuroimaging. Intra-axial susceptibility abnormalities (29/39, 74%, 95%-CI 58–87%) and leukoencephalopathy (18/41, 44%) was common. We observed ischemic/macrophemorrhagic manifestations but vascular and perfusion imaging did not reveal overt pathology. We also observed contrast-enhancement of the parenchyma (3/20, 15%), leptomeninges (3/20, 15%), cranial nerves (2/20, 10%), and spinal nerves 2/4 (50%). At MRI follow-up, regression of leukoencephalopathy and progressive leptomeningeal enhancement were observed in one patient respectively, suggestive of dynamic processes.

The SWI abnormalities and white matter lesions (sometimes with reduced diffusion) both had a striking predilection to the splenium, juxtacortical white matter and long white matter tracts, in line with other recent studies (9,14,18). Their topographical overlap suggests a common cause. Plausible pathophysiological mechanisms may include hypoxia, ischemia,

stasis (with deoxyhemoglobin-rich blood), thrombosis, hemorrhages, inflammation, endothelial injury, or a combination of these (19–21). Interestingly, the corpus callosum is also a predilection site for Susac's syndrome, characterized by autoimmune-mediated occlusions of precapillary arterioles due to endothelial autoantigens (22). The distribution of SWI abnormalities is also reminiscent of previous reports in thrombotic thrombocytopenic purpura (23), critical illness (24), H1N1-influenza with extracorporeal membrane oxygenation (ECMO)-treatment (25), high-altitude sickness (26), cerebral malaria (27), and hepatic encephalopathy (28). In our sample, only 1/10 ECMO-treated patients underwent brain MRI; that person had SWI abnormalities but with a low microbleed anatomical rating scale (MARS) score of 2.

While some SWI abnormalities may be punctate (17), many had a non-spherical shape, suggestive of pathology along vessels or microstructure, as also pointed out by others (18). Endotheliopathy, microthrombosis, and microinfarction have been demonstrated in peripheral organs in COVID-19 (20,29,30). Recent neuropathology in COVID-19 has shown hypoxic injuries and inflammatory changes (19) but also frequent microthrombosis (21). Meanwhile, an *ex vivo in situ* MRI study in COVID-19 showed SWI abnormalities but did not provide histopathological correlates (31). While SWI abnormalities are often referred to as "microbleeds" in radiological reporting, the non-spherical shape of the SWI abnormalities along with evidence for microthrombosis in COVID-19 in other organs and the brain (21,32), suggests that "microbleeds" may be a misnomer in COVID-19. This is supported by the relatively low rate of macroscopic hemorrhages in our study and previous studies (2,12,13), despite routine use of anticoagulation/antiplatelet treatment in COVID-19. Interestingly, hemorrhagic components are not always histopathologically evident in critically ill patients with SWI abnormalities either (33). The terminology may affect the clinical cost-benefit analysis of anticoagulation therapy and since microthrombi is a valid differential diagnosis, this semantic issue is of clinical importance.

The timing of our MRI scans, often in a late disease stage, may contribute to the relatively low frequency of diffusion and perfusion abnormalities. This is supported by the lack of dynamics in intra-axial SWI abnormalities at follow-up, indicating that the microvascular pathologic processes had already waned. The leukoencephalopathic changes in patients with severe COVID-19 seem to have a dynamic nature; the partial resolution of the white matter changes in one case correlated with clinical improvement. Progression of leptomeningeal contrast-enhancement did not correlate with clinical deterioration in another. Similar leptomeningeal enhancement has previously been reported in multiple sclerosis (34), and oligoclonal bands (though matched in serum) have been reported in COVID-19 with leptomeningeal enhancement (10,14). While nonspecific, these findings in combination with neuroinflammatory disorders being linked to previous coronaviruses (1,2), hint that neuroinflammatory complications of COVID-19 may occur.

Anosmia is common in COVID-19 (2), and olfactory bulb MRI signal abnormalities have indeed been described (35). Such findings were relatively rare in our study, but their visual assessment can often be equivocal. The presence of prominent subarachnoid spaces around the optic nerves was common (20/43, 47%) and raises potential questions about intracranial pressure in COVID-19. In 4 patients (3 intubated, 1 tracheostomy), this finding could possibly

be confounded by positive pressure ventilation. Lumbar punctures were rarely performed, due to contraindications.

Our study has some limitations. First, as with all retrospective studies, it is subject to systematic confounders. Our patients had varying degrees of disease severity, from completely asymptomatic with incidental PCR-positivity to critically ill patients. There naturally exists an indication bias, whereby MRI was performed almost exclusively in severely ill patients. Second, the lack of a control group limits the possibility to draw conclusions on the specificity of our findings to COVID-19. Third, the lack of histopathological data is also a limitation. Fourth, the retrospective nature of this study and the commonly impaired consciousness of the patients limited the ability to perform clinico-radiological correlations, such as olfactory/taste symptomatology. Fifth, the standardized protocol did not include coronal T2-weighted or short tau inversion recovery imaging, which would have been a good complement for assessing the olfactory bulbs. Sixth, the limited number of follow-up MRIs and short observation period does not allow any meaningful conclusions about the long-term clinical outcomes.

In conclusion, brain MRI is essential in order to depict the oftentimes subtle vascular and inflammatory aspects of nervous system involvement in patients hospitalized with COVID-19. The ovoid shape of the susceptibility abnormalities bears similarities to other conditions characterized by endotheliopathy and microthrombosis, both observed in other organs in severe COVID-19. While longitudinal data is limited, the regression of leukoencephalopathy and concurrent clinical improvement in one of our patients is encouraging. The common presence of prominent subarachnoid spaces around the optic nerves raises potential questions about intracranial pressure in COVID-19 and should be evaluated in future studies.

### Acknowledgments

We would like to thank our colleagues at the Department of Neuroradiology for making this study possible and for their valuable input. We would especially like to acknowledge the contributions of Jessica Bystam, Per Grane, Jens Kolloch, Ola Norbeck, Harriet Nyström, Fredrik Piehl Anna Sjöström and Adrian Szum. We thank Ioannis Koupidis for his help with figure panels. We also want to thank all of our clinical colleagues that have worked so tirelessly and bravely during this pandemic. Finally, we would like to thank all the patients and their families.

### Funding

RO was supported by MultipleMS (EU Horizon 2020 grant 733161) and COMBAT-MS (Patient-Centered Outcomes Research Institute grant MS-1511–33196). JL was supported by grants from the Stockholm Region Clinical Postdoc program and a private donation by Tedde Jeansson Sr. AFD was supported by grants provided by the Stockholm Region (ALF project). TG was supported by grants from the Stockholm Region Clinical Postdoc program, Stockholm Region ALF and StratNeuro.

### References

1. Zubair AS, McAlpine LS, Gardin T, Farhadian S, Kuruvilla DE, Spudich S. Neuropathogenesis and Neurologic Manifestations of the Coronaviruses in the Age of Coronavirus Disease 2019: A Review. *JAMA Neurol.* 2020.

2. Román GC, Spencer PS, Reis J, et al. The neurology of COVID-19 revisited: A proposal from the Environmental Neurology Specialty Group of the World Federation of Neurology to implement international neurological registries. *J Neurol Sci.* 2020;414:116884.
3. Mao L, Jin H, Wang M, et al. Neurologic Manifestations of Hospitalized Patients With Coronavirus Disease 2019 in Wuhan, China. *JAMA Neurol.* 2020;77(6):683–690.
4. Asadi-Pooya AA, Simani L. Central nervous system manifestations of COVID-19: A systematic review. *J Neurol Sci.* 2020;413:116832.
5. Oxley TJ, Mocco J, Majidi S, et al. Large-Vessel Stroke as a Presenting Feature of Covid-19 in the Young. *New England Journal of Medicine.* 2020;0(0):e60.
6. Kansagra AP, Goyal MS, Hamilton S, Albers GW. Collateral Effect of Covid-19 on Stroke Evaluation in the United States. *New England Journal of Medicine.* 2020.
7. Poyiadji N, Shahin G, Noujaim D, Stone M, Patel S, Griffith B. COVID-19-associated Acute Hemorrhagic Necrotizing Encephalopathy: CT and MRI Features. *Radiology.* 2020;201187.
8. Moriguchi T, Harii N, Goto J, et al. A first case of meningitis/encephalitis associated with SARS-CoV-2. *Int J Infect Dis.* 2020;94:55–58.
9. Sachs JR, Gibbs KW, Swor DE, et al. COVID-19-Associated Leukoencephalopathy. *Radiology. Radiological Society of North America;* 2020;201753.
10. Helms J, Kremer S, Merdji H, et al. Neurologic Features in Severe SARS-CoV-2 Infection. *New England Journal of Medicine.* 2020;382(23):2268–2270.
11. More on Neurologic Features in Severe SARS-CoV-2 Infection. *New England Journal of Medicine.* 2020;382(26):e110.
12. Kandemirli SG, Dogan L, Sarikaya ZT, et al. Brain MRI Findings in Patients in the Intensive Care Unit with COVID-19 Infection. *Radiology.* 2020;201697.
13. Mahammed A, Saba L, Vagal A, et al. Imaging in Neurological Disease of Hospitalized COVID-19 Patients: An Italian Multicenter Retrospective Observational Study. *Radiology.* 2020;201933.
14. Kremer S, Lersy F, de Sèze J, et al. Brain MRI Findings in Severe COVID-19: A Retrospective Observational Study. *Radiology.* 2020;202222.
15. Gregoire SM, Chaudhary UJ, Brown MM, et al. The Microbleed Anatomical Rating Scale (MARS): reliability of a tool to map brain microbleeds. *Neurology.* 2009;73(21):1759–1766.
16. Chung MS, Choi WR, Jeong H-Y, Lee JH, Kim JH. MR Imaging-Based Evaluations of Olfactory Bulb Atrophy in Patients with Olfactory Dysfunction. *Am J Neuroradiol.* 2018;39(3):532–537.
17. Radmanesh A, Derman A, Lui YW, et al. COVID-19 –associated Diffuse Leukoencephalopathy and Microhemorrhages. *Radiology.* 2020;202040.
18. Fitsiori A, Pugin D, Thieffry C, Lalive P, Vargas MI. Unusual Microbleeds in Brain MRI of Covid-19 Patients. *Journal of Neuroimaging.* 2020.
19. Solomon IH, Normandin E, Bhattacharyya S, et al. Neuropathological Features of Covid-19. *New England Journal of Medicine.* 2020.
20. Varga Z, Flammer AJ, Steiger P, et al. Endothelial cell infection and endotheliitis in COVID-19. *The Lancet.* 2020;395(10234):1417–1418.
21. Bryce C, Grimes Z, Pujadas E, et al. Pathophysiology of SARS-CoV-2: targeting of endothelial cells renders a complex disease with thrombotic microangiopathy and aberrant immune response. *The Mount Sinai COVID-19 autopsy experience. medRxiv.*

2020;2020.05.18.20099960.

22. Dörr J, Krautwald S, Wildemann B, et al. Characteristics of Susac syndrome: a review of all reported cases. *Nat Rev Neurol*. 2013;9(6):307–316.
23. Noorbakhsh-Sabet N, Zand R. Thrombotic Thrombocytopenic Purpura with Concomitant Progressive Cerebral Microbleeds. *Journal of Stroke and Cerebrovascular Diseases*. 2016;25(11):e214–e215.
24. Fanou EM, Coutinho JM, Shannon P, et al. Critical Illness-Associated Cerebral Microbleeds. *Stroke*. 2017;48(4):1085–1087.
25. Chow FC, Edlow BL, Frosch MP, Copen WA, Greer DM. Outcome in Patients with H1N1 Influenza and Cerebrovascular Injury Treated with Extracorporeal Membrane Oxygenation. *Neurocrit Care*. 2011;15(1):156–160.
26. Hackett PH, Yarnell PR, Weiland DA, Reynard KB. Acute and Evolving MRI of High-Altitude Cerebral Edema: Microbleeds, Edema, and Pathophysiology. *Am J Neuroradiol*. 2019;40(3):464–469.
27. Nickerson JP, Tong KA, Raghavan R. Imaging cerebral malaria with a susceptibility-weighted MR sequence. *Am J Neuroradiol*. 2009;30(6):e85-86.
28. Achiriloaei AF, Kido D, Wycliffe D, Jacobson JP. White Matter Microsusceptibility Changes in Patients With Hepatic Encephalopathy. *J Radiol Case Rep*. 2011;5(8):1–7.
29. Wichmann D, Sperhake J-P, Lütgehetmann M, et al. Autopsy Findings and Venous Thromboembolism in Patients With COVID-19. *Annals of Internal Medicine*. American College of Physicians; 2020.
30. Xu P, Zhou Q, Xu J. Mechanism of thrombocytopenia in COVID-19 patients. *Ann Hematol*. 2020;1–4.
31. Coolen T, Lolli V, Sadeghi N, et al. Early postmortem brain MRI findings in COVID-19 non-survivors. *Neurology*. 2020.
32. Ackermann M, Verleden SE, Kuehnel M, et al. Pulmonary Vascular Endothelialitis, Thrombosis, and Angiogenesis in Covid-19. *New England Journal of Medicine*. Massachusetts Medical Society; 2020.
33. Chang J, Arani K, Chew S, et al. Susceptibility Etching on MRI in Patients with Microangiopathy. *J Neuroimaging*. 2017;27(1):43–49.
34. Absinta M, Vuolo L, Rao A, et al. Gadolinium-based MRI characterization of leptomeningeal inflammation in multiple sclerosis. *Neurology*. 2015;85(1):18–28.
35. Politi LS, Salsano E, Grimaldi M. Magnetic Resonance Imaging Alteration of the Brain in a Patient With Coronavirus Disease 2019 (COVID-19) and Anosmia. *JAMA Neurol*. 2020.

**Table 1. Standardized Brain MRI Protocol.**

<b>COVID-19 brain MRI protocol without GBCA</b>	<b>COVID-19 brain MRI protocol with GBCA</b>
Sagittal 3D T <sub>2</sub> -weighted FLAIR	Sagittal 3D T <sub>2</sub> -weighted FLAIR
Axial 3D SWI	Axial 3D SWI
Axial 2D DWI	Axial 2D DWI
Axial 2D T <sub>2</sub> -weighted imaging	Sagittal 3D T <sub>1</sub> -weighted TSE
Sagittal 3D T <sub>1</sub> -weighted GRE IR	Dynamic susceptibility contrast perfusion
Sagittal 3D T <sub>1</sub> -weighted TSE	Axial 2D T <sub>2</sub> -weighted imaging with GBCA
Arterial TOF MRA	Sagittal 3D T <sub>1</sub> -weighted GRE IR with GBCA
ASL perfusion	Sagittal 3D T <sub>1</sub> -weighted TSE with GBCA
	Sagittal 3D T <sub>2</sub> -weighted FLAIR with GBCA
	Arterial TOF MRA

*ASL = arterial spin labeling, COVID-19 = coronavirus disease 2019, DWI = diffusion-weighted imaging, GBCA = gadolinium-based contrast agent, GRE IR = gradient-recalled echo with inversion recovery, FLAIR = fluid-attenuated inversion recovery, SWI = susceptibility-weighted imaging, TOF MRA = time-of-flight magnetic resonance angiography, TSE = turbo spin echo. Detailed sequence parameters are found in Table E1.*

**Table 2. Demographics of Study Patients.**

	<b>Number of patients (n=185)</b>
<b>Mean Age in years (standard deviation, range)</b>	62 (14, 19 – 95)
Number of men	138 (75%)
<b>No. of deceased patients (%)</b>	46 (25%)
No of deceased patients who were men (%)	38 (83%)
<b>Body mass index, mean (range)</b>	28 (17 – 46)
<b>Hypertension No. of patients (%)</b>	87 (47%)
<b>Diabetes mellitus Type 1</b>	2 (1.1%)
<b>Diabetes mellitus Type 2</b>	48 (26%)
<b>No. of patients needing ventilator support (%)</b>	115 (62%)
No of ventilator patients who were men (%)	102 (89%)
<b>Days on ventilator, mean (range)</b>	19 (0 – 46)
<b>Days from symptom onset to intubation, mean (range)</b>	12 (0 – 61)
<b>No. of patients requiring ECMO support (%)</b>	10 (5.4%)
No of ECMO patients who were men (%)	9 (90%)
<b>Days on ECMO, mean (range)</b>	16 (4 – 47)
Days from intubation to ECMO, mean (range)	7 (2 – 23)
<b>ARDS grade - none, mild, moderate, severe</b>	57 (31%), 11 (6%), 40 (22%), 76 (41%)
<b>No. of patients with pulmonary thromboembolism</b>	33 (18%)
<b>Imaging Modality</b>	
No. of patients examined with brain CT (%)	174 (94%)
No. of patients examined with brain MRI (%)	43 (23%)
No. of patients examined with both brain CT and MRI (%)	32 (17%)
No. of patients examined with spinal MRI (%)	7 (3.8%)

\*One patient died before making it to the ICU and from the available data it was impossible to calculate the ARDS grade. ARDS = Adult Respiratory Distress Syndrome, CRRT = Continuous Renal Replacement Therapy, ECMO = Extracorporeal Membrane Oxygenation.

**Table 3. CT Findings.**

	<b>Number of patients</b>
<b>Days from symptom start to scan</b>	
• Median (range)	21 (0 – 73)
<b>Hemorrhages</b>	
• All	16 (9.2%, 95%-CI 5.4 – 15%)
• Intracerebral	8 (4.6%, 95%-CI 2.0 – 8.9%)
• Intracerebellar	3 (1.7%, 95%-CI 0.36 – 5.0%)
• Subarachnoid	5 (2.9%, 95%-CI 0.94 – 6.6%)
• Subdural	8 (4.6%, 95%-CI 2.0 – 8.9%)
• Epidural	2 (1.1%, 95%-CI 0.14 – 4.1)
<b>Ischemia</b>	
• All	34 (20%, 95%-CI 14 – 26%)
• Acute cortical infarct	11 (6.3%, 95%-CI 3.2 – 11%)
• Chronic cortical infarct	12 (6.9%, 95%-CI 3.6 – 12%)
• Acute lacunar infarct	4 (2.3%, 95%-CI 0.63 – 5.8%)
• Chronic lacunar infarct	13 (7.5%, 95%-CI 4.0 – 12%)

*Findings reported on a per-patient basis, based on the 174 patients that underwent brain CT.*

**Table 4. MRI Findings.**

	<b>Number of patients</b>
<b>Days from symptom start to scan</b> Median (range)	34 (6 – 78)
<b>Hemorrhage, all</b>	11/39 (28%, 95%-CI 15 – 45%)
• Intracerebral	1/39 (2.6%, 95%-CI 0.06 – 13%)
• Intracerebellar	1/39 (2.6%, 95%-CI 0.06 – 13%)
• Subarachnoid	9/39 (23%, 95%-CI 11 – 39%)
<b>SWI abnormalities, all</b>	29/39 (74%, 95%-CI 58 – 87%)
• Corpus callosum	23/39 (59%, 95%-CI 42 – 74%)
• Juxtacortical	14/39 (36%, 95%-CI 21 – 53%)
• Cortical superficial siderosis	3/39 (7.7%, 95%-CI 1.6 – 21%)
<b>Ischemia, all</b>	10/42 (24%, 95%-CI 12 – 39%)
• Acute cortical infarct	5/41 (12%, 95%-CI 4.1 – 26%)
• Chronic cortical infarct	4/42 (9.5%, 95%-CI 2.7 – 23%)
• Acute lacunar infarct	5/41 (12%, 95%-CI 4.1 – 26%)
• Chronic lacunar infarct	3/42 (7.1%, 95%-CI 1.5 – 19%)
<b>White matter changes, all</b>	23/41 (56%, 95%-CI 40 – 72%)
• Periventricular	18/41 (44%, 95%-CI 28 – 60%)
• Juxtacortical	10/41 (24%, 95%-CI 12 – 40%)
• Middle cerebellar peduncles	7/41 (17%, 95%-CI 7.2 – 32%)
• Corpus callosum	11/41 (27%, 95%-CI 14 – 43%)
• Cytotoxic lesion in the corpus callosum	1/41 (2.4%, 95%-CI 0.06 – 13%)
• White matter changes with reduced DWI*	1/41 (2.4%, 95%-CI 0.06 – 13%)
<b>Contrast enhancement</b>	
• Intra-axial	3/20 (15%, 95%-CI 3.2 – 38%)
• Leptomeningeal	3/20 (15%, 95%-CI 3.2 – 38%)
• Cranial nerves	2/20 (10%, 95%-CI 1.2 – 32%)
• Spinal nerves	2/4 (50%, 95%-CI 6.8 – 93%)
<b>Vessel wall enhancement</b>	6/17 (35%, 95%-CI 14 – 62%)
<b>Abnormalities on arterial 3D TOF MRA</b>	**

Prominent optic nerve subarachnoid spaces	20/36 (56%, 95%-CI 38 – 72%)
Abnormally high T2 signal in olfactory bulb	7/37 (19%, 95%-CI 8.0 – 35%)

All results given as number of patients / number of patients with appropriate imaging for the finding with corresponding percentages in parentheses. Some patients were excluded from the respective analyses because of severe motion artifacts or lack of acquisition, such as post-contrast imaging.

\*Findings raising suspicion of posterior reversible encephalopathy syndrome, hypoxic/metabolic changes, or encephalitis.

\*\*A few elderly patients had evidence of atheromatous changes in the cerebral vessels.

DWI = diffusion-weighted imaging, SWI = susceptibility-weighted imaging, TOF MRA = time-of-flight magnetic resonance angiography.

## Figure Legends

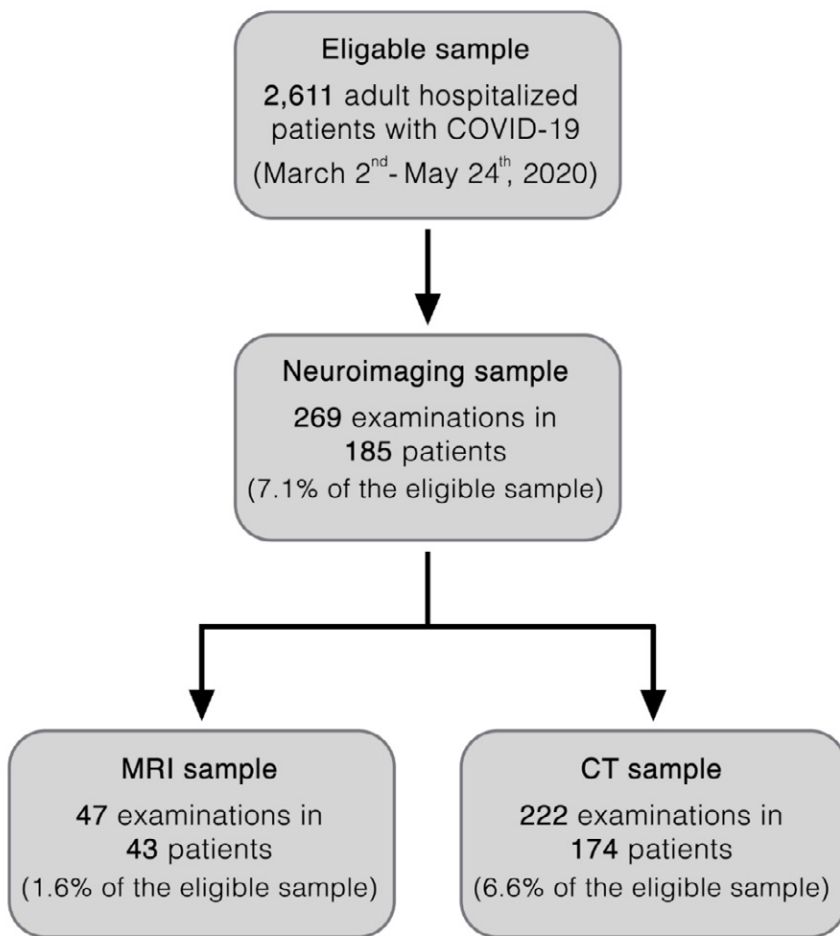


**Figure 1.** Flow chart of the study. Inclusion criteria were: Positive polymerase-chain-reaction test result for severe acute respiratory syndrome coronavirus 2; age of  $\geq 18$  years; neuroimaging performed during the study period. No exclusion criteria were applied to ensure a complete consecutive study sample.

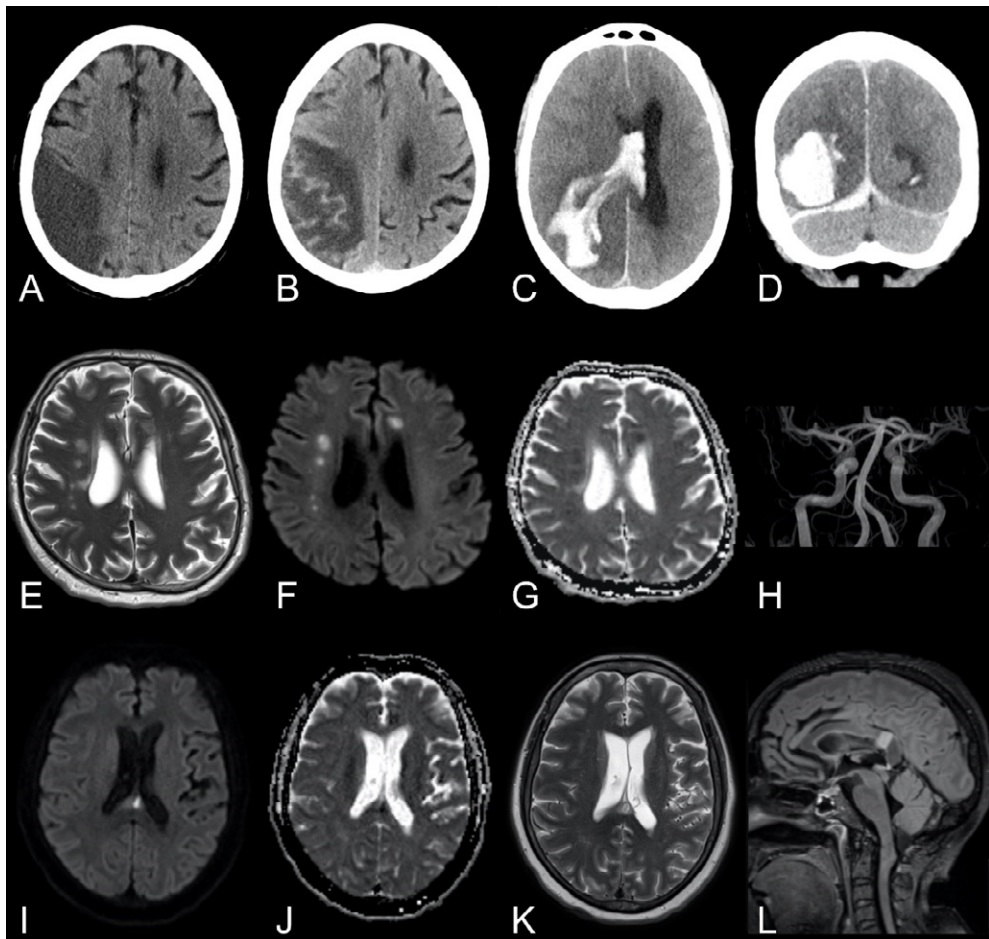


**Figure 2.** Macrovascular and diffusion imaging findings.

**First row (A, B):** Man in his late 60s with COVID-19, left side motor symptoms and left-sided ophthalmoplegia upon a routine wake up test from anesthesia. A, Non-enhanced brain CT in the axial view demonstrating an infarct of the right middle cerebral artery territory. B, Axial non-enhanced brain CT in the axial view a week later revealed hemorrhagic transformation.

**First row (C, D):** Man in his mid-50s with COVID-19 a month after symptom onset and several weeks in the ICU. Non-enhanced brain CT in the, C, axial and, D, coronal views. Intracerebral hematoma dissecting into the ventricles and along the right tentorium. Low attenuation in the territories of right middle and posterior cerebral arteries were also found.

**Second row:** Man in his mid-50s with COVID-19 after a month in the ICU and impaired consciousness (GCS 3) after termination of anesthesia. Brain MRI with, E, axial T<sub>2</sub>-weighted imaging, F, b1000 DWI, and, G, ADC map showing multiple, bilateral acute lacunar infarcts in the semioval centers. H, TOF MRA with normal findings.

**Third row:** Woman in her late 40s with COVID-19, impaired consciousness and paretic extremities 2 weeks after admission to the ICU. Brain MRI with, I, axial b1000 DWI, J, ADC map, K, T<sub>2</sub>-weighted imaging, and, L, sagittal T<sub>2</sub>-weighted FLAIR showed a cytotoxic lesion of the corpus callosum in the splenium.

ADC = apparent diffusion coefficient, DWI = diffusion weighted imaging, FLAIR = fluid-attenuated inversion recovery, GCS = Glasgow coma scale, ICU = intensive care unit, SWI = susceptibility-weighted imaging, TOF MRA = time-of-flight magnetic resonance angiography.

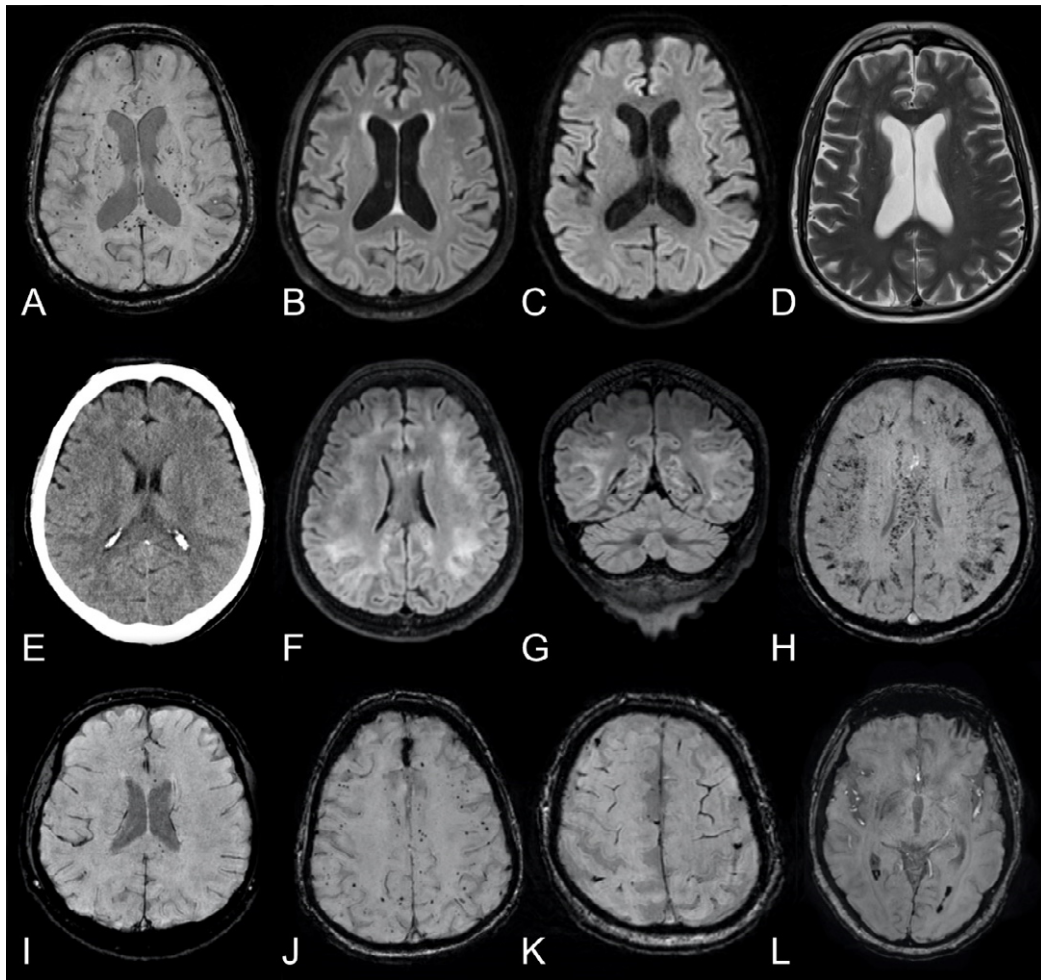


**Figure 3.** SWI abnormalities.

**First row:** Man in his mid 60s with COVID-19, tetraplegia and prolonged confusion (GCS14) after extubation. Brain MRI with, *A*, axial SWI reveals numerous cerebral susceptibility abnormalities bilaterally in the white matter, most prominently in the corpus callosum and especially in the splenium, many of which have an ovoid shape (as further exemplified in Figure E3). *B*, Axial T<sub>2</sub>-weighted FLAIR, *C*, b1000 DWI, and, *D*, T<sub>2</sub>-weighted imaging without any remarkable findings.

**Second row:** Man in his early 60s with COVID-19 and impaired consciousness (GCS 2+T+1) a week after termination of anesthesia. *E*, Non-enhanced brain CT in the axial view initially reported as normal. Brain MRI the following day with T<sub>2</sub>-weighted FLAIR images in the, *F*, axial and, *G*, coronal views showing subcortical extension of leukoencephalopathy without associated reduced diffusion (images not shown). *H*, Axial SWI reveals extensive susceptibility abnormalities with a predilection for subcortical U-fibers, corticospinal tracts, and the corpus callosum.

**Third row:** Four other patients with COVID-19. Brain MRI with SWI in the axial view showing different degrees and types of susceptibility changes. A few susceptibility abnormalities in the splenium and genu of corpus callosum (*I*, man in his mid 60s), numerous subcortical cerebral susceptibility artifacts (*J*, man in his mid 60s), subarachnoid hemorrhage and cortical superficial siderosis (*K*, man in his late 50s) and dependent intraventricular blood in the posterior horns of the lateral ventricles (*L*, woman in her mid 40s).

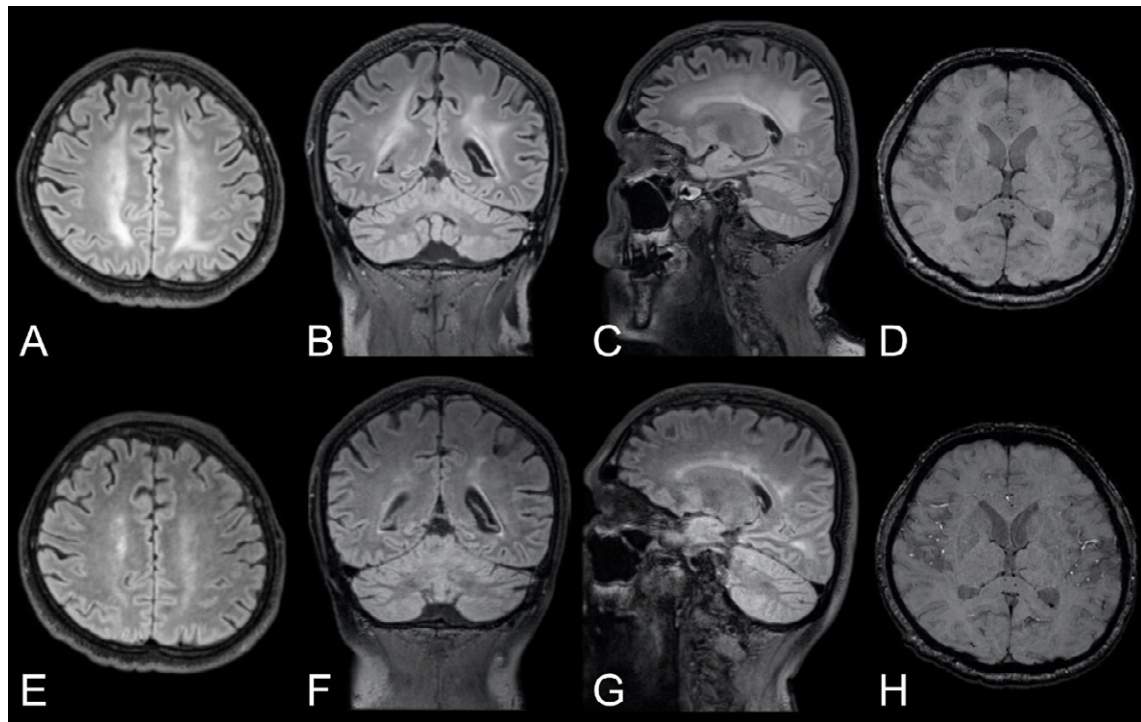


**Figure 4.** Longitudinal changes in white matter signal abnormalities.

**Top row:** Man in his mid 40s with COVID-19 and confusion a month after symptom onset and 2 weeks in the ICU. A-C, Baseline brain MRI with non-enhanced T<sub>2</sub>-weighted FLAIR images in the axial, coronal, and sagittal views exhibit symmetric confluent white matter changes bilaterally. D, Axial SWI also revealed a few susceptibility abnormalities in the splenium of corpus callosum. There was no reduced diffusion (images not shown). EEG performed 3 days prior to the MRI, found signs of encephalopathy.

**Bottom row:** E-G, Follow-up brain MRI a week later with non-enhanced T<sub>2</sub>-weighted FLAIR images in the same views demonstrating partial resolution of the leukoencephalopathy, correlating with an improved mental state. H, The extent of susceptibility abnormalities in the brain parenchyma was unchanged.

FLAIR = fluid-attenuated inversion recovery, ICU = intensive care unit, SWI = susceptibility-weighted imaging.

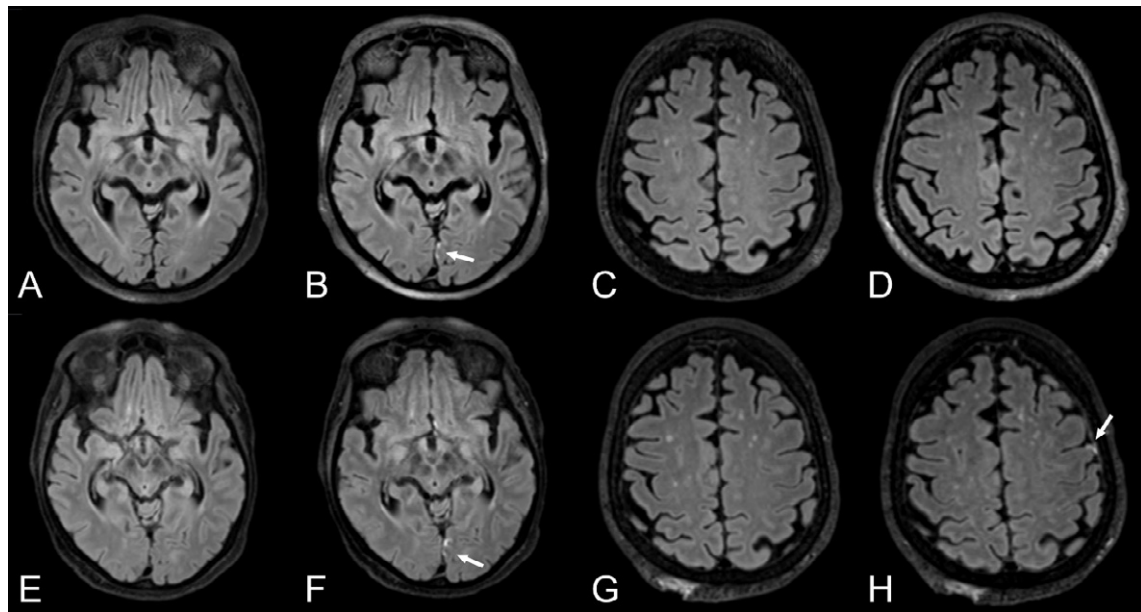


**Figure 5.** Progressive leptomeningeal enhancement.

**Top row:** Woman in her late 60s with COVID-19 with impaired consciousness after termination of anesthesia. Baseline brain MRI with, *A*, pre- and, *B*, post-contrast T<sub>2</sub>-weighted FLAIR images in the axial view revealing a solitary focus of leptomeningeal enhancement (arrow) along the medial aspect of the left occipital lobe.

**Bottom row:** Follow-up 3.5 weeks later. The original leptomeningeal enhancement focus had increased slightly (*E*, *F* with arrow). A new focus of leptomeningeal enhancement had formed along the left inferior frontal gyrus (*G*, *H* with arrow) not present on the baseline scan (*C*, *D*). FLAIR = fluid-attenuated inversion recovery, ICU = intensive care unit.

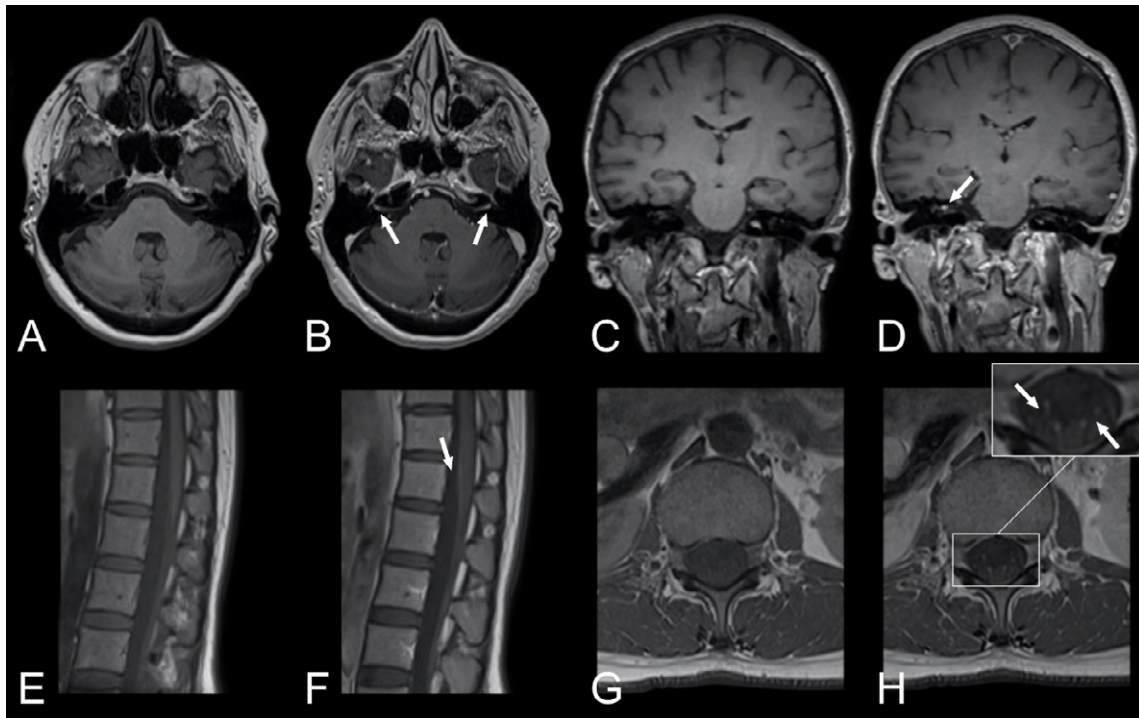


**Figure 6.** Cranial nerve and spinal nerve root enhancement.

**First row (A, B):** Woman in her early 60s with COVID-19, bilateral leg weakness and paresthesias. Brain MRI with T<sub>1</sub>-weighted images, A, pre- and, B, post-contrast in the axial view showing focal contrast enhancement of the canalicular segment of facial nerve bilaterally. Lumbar puncture showed elevated albumin with no cells and nerve conduction studies were consistent with acute demyelinating polyneuropathy. She received intravenous immunoglobulin treatment on suspicion of Guillain-Barré syndrome and improved clinically.

**First row (C, D):** Woman in her mid 40s with COVID-19 and typical findings of right-sided vestibular neuritis. Brain MRI with T<sub>1</sub>-weighted images, C, pre- and, D, post-contrast in the coronal view depicting focal enhancement of the right vestibular nerve.

**Second row:** Woman in her mid 30s with COVID-19, pain in the lumbar region and paresthesias in the lower extremities. Lumbar spinal MRI with T<sub>1</sub>-weighted images, E, pre- and, F, post-contrast in the sagittal view revealed faint contrast enhancement along the cauda equina. T<sub>1</sub>-weighted images, G, pre- and, H, post-contrast in the axial view verified contrast enhancement of the nerve roots.

**Table E1. Technical MRI Parameters**

GE Optima MR450W GEM 1.5 Tesla	T2 FLAIR				DWI	DSC Perfusion	MRA 3D TOF	MRA 2D INHANCE venous
	T1 BRAVO	T1 CUBE	CUBE	T2 TSE PROPELLER			arterial	
Sequence type	3D GRE	3D TSE	3D TSE	2D TSE Motion corrected	3D EPI	2D EPI	MRA	MRA
Acquisition plane	Axial	Sagittal	Sagittal	Axial	Axial	Axial	Axial	Sagittal
Phase encoding direction	R >> L	A >> P	A >> P	R >> L	A >> P	A >> P	R >> L	A >> P
Repetition time (ms)	8.2	550	7600	4050	89.4	7638	1500	24
Echo time (ms)	3.1	12	120	100	36.5	76.6/169	30	2.5
Inversion time (ms)	450	N/A	2059	N/A	N/A	N/A	N/A	N/A
Field of view (mm)	240	256	256	240	240	240	200	240
Matrix size	240	256	224	340	320	128	96	320x240
Slice thickness (mm)	1.2	1	1.6	3	2	4	4	0.8
In-plane resolution (mm)	1x1	1x1	1.1x1.1	0.7x0.7	0.8x0.8	1.9x1.9	2.5x2.5	0.7x0.8
Distance factor	0	0	0	0	0	0	0	-12%
Slices	150	182	116	51	80	37	21	40 per slab
Phase oversampling	0	0	0	0	0	0	0	0
Turbo/EPI factor	N/A	22	180	30	16	64	48	N/A
Bandwidth (Hz/px)	260.4	488.3	372.1	294.1	521	3906	5208	208.3
iPAT (GRAPPA factor. reference lines))	1.5/1	2	2/2	2	N/A	2/1	2/1	2
Flip angle (°)	12	Variable	Variable	142 (Variable)	20	90 & 180	60	20
Averages (N)	1	1	1	2.5	1	2	1	1
Slabs (N)	1	1	1	N/A	1	N/A	N/A	3
Fat Suppression	None	None	Fat, darkest	None	Excitation	Excitation	None	Fat
Scan time (min:sec)	03:50	04:40	04:45	03:39	01:34	01:55	01:15	06:41

Philips Ingenia 1.5 Tesla	T2 FLAIR				
	T1 BrainView	BrainView	T2 TSE MultiVane XD	SWIp	DWI
Sequence type	3D TSE	3D TSE	2D TSE Motion corrected	3D GRE	2D EPI
Acquisition plane	Axial	Sagittal	Axial	Axial	Axial
Phase encoding direction	AP	AP	n/a	RL	AP
Repetition time (ms)	600	4800	4000	52	2953
Echo time (ms)	29	300	110	0	90
Inversion time (ms)	n/a	1660	n/a	n/a	n/a
Field of view (mm)	250	250	230	230	230
Matrix size	640 (acquired 252x250)	400 (208x209)	528 (384)	672 (272)	176 (144x90)
Slice thickness (mm)	1.1	1.2	5	2	5
In-plane resolution (mm)	0.39 (acquired 1)	0.625 (1.2)	0.44 (0.6)	0.34 (0.85)	1.3 (1.6x2.6)

Distance factor	-50%	-50%	10%	-50%	10%		
Slices	327	328	22	260	22		
Phase oversampling	0%	0%	0%	0%	0%		
Turbo/EPI factor	20	116	30	4	45		
Bandwidth (Hz/px)	352	426	218	134	1387		
Flip angle (°)	90	90	90	20	90		
Averages (N)	1	1	1	1	1		
Slabs (N)	1	1	1	1	1		
Fat Suppression	Fat sat	Fat sat	Fat sat	No	Fat sat		
Scan time (min:sec)	3:25	3:02	2:24	3:33	0:34		

Siemens Aera 1.5 Tesla	T1 MPRAGE		T2 FLAIR SPACE		T2 TSE BLADE		SWI	DWI RESOLVE	DSC Perfusion	MRA 3D TOF	MRA 2D TOF
	T1 MPRAGE	T1 SPACE	SPACE	2D TSE Motion	corrected	3D GRE	2D EPI	2D EPI	arterial	venous	
Sequence type	3D GRE	3D TSE	3D TSE	2D TSE Motion	corrected	3D GRE	2D EPI	2D EPI	MRA	MRA	
Acquisition plane	Sagittal	Sagittal	Sagittal	Axial	Axial	Axial	Axial	Axial	Axial	Sagittal	
Phase encoding direction	A >> P	A >> P	A >> P	A >> P	A >> P	R >> L	A >> P	A >> P	R >> L	A >> P	
Repetition time (ms)	1900	500	5000	3570	49	9320	2000	2000	24	24	
Echo time (ms)	2.67	7.2	333	99	40	69/112	30	30	7	7	
Inversion time (ms)	1100	N/A	1600	N/A	N/A	N/A	N/A	N/A	N/A	N/A	
Field of view (mm)	250	250	260	240	230	230	230	230	180	250	
Matrix size	256	256	256	320	256	192	128	128	256	256	
Slice thickness (mm)	1	1	1	3	2	4	4	4	0.5	3	
In-plane resolution (mm)	1x1	1x1	1x1	0.8x0.8	0.9x0.9	1.2x1.2	1.8x1.8	1.8x1.8	0.4x0.4	1x1	
Distance factor	50%	0%	0%	0%	20%	0%	30%	30%	-18%	-33%	
Slices	192	176	176	52	72	39	25	25	44	75	
Phase oversampling	0%	0%	0%	0%	0%	0%	0%	0%	0%	0%	
Turbo/EPI factor	196	36	242	35	N/A	96	0/128	0/128	N/A	N/A	
Bandwidth (Hz/px)	150	630	592	365	80	814	1502	1502	100	90	
iPAT (GRAPPA factor, reference lines))	2/24/1	2/24/1	2	N/A	2/24/1	2/96	2/40	2/32/1	2/24		
Flip angle (°)	15	T1 Variable	T2 variable	121	15	180	90	25	60		
Averages (N)	1	1	1	1	1	1	1	1	1	1	
Slabs (N)	1	1	1	N/A	1	N/A	N/A	N/A	4	N/A	
Fat Suppression	None	None	Fat. strong	None	None	Fat. strong	Fat. Sat	Fat. Sat	None	None	
Scan time (min:sec)	04:18	04:39	05:07	02:53	04:29	04:13	04:13	04:13	05:16	03:38	

Siemens Skyra 3 Tesla	T1 MPRAGE		T2 FLAIR SPACE		T2 TSE BLADE		SWI	DWI RESOLVE	DSC Perfusion	MRA 3D TOF	MRA 2D TOF
	T1 MPRAGE	T1 SPACE	SPACE	2D TSE Motion	corrected	3D GRE	2D EPI	2D EPI	arterial	venous	
Sequence type	3D GRE	3D TSE	3D TSE	2D TSE Motion	corrected	3D GRE	2D EPI	2D EPI	MRA	MRA	
Acquisition plane	Sagittal	Sagittal	Sagittal	Axial	Axial	Axial	Axial	Axial	Axial	Sagittal	
Phase encoding direction	A >> P	A >> P	A >> P	A >> P	A >> P	R >> L	A >> P	A >> P	R >> L	A >> P	
Repetition time (ms)	1900	450	5000	6250	28	8300	3500	3500	21	20	

Echo time (ms)	02.29	4.7	386	117	22	64/100	28	03.42	05.23
Inversion time (ms)	900	N/A	1600	N/A	N/A	N/A	N/A	N/A	N/A
Field of view (mm)	240	256	256	220	220	220	220	200	250
Matrix size	256	256	256	320	256	160	128	384	256
Slice thickness (mm)	1	1	1	3	2	4	4	0.5	2.5
In-plane resolution (mm)	0.9x0.9	1x1	1x1	0.7x0.7	0.9x0.9	1.4x1.4	1.7x1.7	0.5x0.5	1x1
Distance factor	50%	0%	0%	0%	20%	0%	0%	-20%	-33%
Slices	208	176	160	54	72	41	41	40 per slab	85
Phase oversampling	0%	0%	0%	0%	0%	0%	0%	0%	0%
Turbo/EPI factor	240/0	44/0	278/0	28/0	N/A	0/80	0/128	N/A	N/A
Bandwidth (Hz/px)	200	434	751	363	120	919	1562	186	201
iPAT (GRAPPA factor. reference lines))	2/24/1	2	2/24/1		2/8	2/24/1	2/80	2/40	2/32/1
Flip angle (°)	8	T1 Variable	T2 variable	90	15	180	90	18	60
Averages (N)	1	1.8	1	1	1	1	1	1	1
Slabs (N)	1	1	1	N/A	1	N/A	N/A	4	1
Fat Suppression	None	None	Fat. strong	None	None	Fat. strong	Fat	None	None
Scan time (min:sec)	04:26	05:05	04:52	02:19	04:37	02:31	04:16	05:33	04:08

Siemens PrismaFit 3 Tesla	T1 MPRAGE		T2 FLAIR SPACE	T2 TSE BLADE	SWI	DWI RESOLVE	DSC Perfusion	MRA 3D TOF	MRA 2D TOF
	+Gd	T1 SPACE						arterial	venous
Sequence type	3D GRE	3D TSE	3D TSE	2D TSE Motion corrected	3D GRE	2D EPI	2D EPI	MRA	MRA
Acquisition plane	Sagittal	Sagittal	Sagittal	Axial	Axial	Axial	Axial	Axial	Sagittal
Phase encoding direction	A >> P	A >> P	A >> P	A >> P	R >> L	A >> P	A >> P	R >> L	A >> P
Repetition time (ms)	1900	450	5000	5650	28	5220	2730	21	20
Echo time (ms)	02.29	4.7	386	106	20	54/89	28	03.42	05.23
Inversion time (ms)	900	0	1800	0	0	0		0	0
Field of view (mm)	240	256	256	220	220	220	220	200	250
Matrix size	256	256	256	320	256	160	128	384	256
Slice thickness (mm)	1	1	1	3	2	4	4	0.5	2.5
In-plane resolution (mm)	0.9x0.9	1x1	1x1	0.7x0.7	0.9x0.9	1.4x1.4	1.7x1.7	0.5x0.5	1x1
Distance factor	50%	0%	0%	0%	20%	0%	0%	-20%	-33%
Slices	208	176	160	54	72	41	41	40 per slab	85
Phase oversampling	0%	0%	0%	0%	0%	0%	0%	0%	0%
Turbo/EPI factor	240/0	44/0	278	28/0	N/A	0/80	0/128	N/A	N/A
Bandwidth (Hz/px)	200	434	751	363	120	977	1562	186	201
iPAT (GRAPPA factor. reference lines))	2/24/1	2001/2/24	2/24/1	2/8	2/24/1	2/80	2/40	2/32	2/24
Flip angle (°)	8	T1 Variable	T2 variable	90	15	180	90	18	60
Averages (N)	1	1.4	1	1	1	1	1	1	1
Slabs (N)	1	1	1	N/A	1	N/A	N/A	4	N/A
Fat Suppression	None	None	Fat. Strong	None	None	Fat. strong	Fat sat	None	None
Scan time (min:sec)	04:26	04:21	04:52	02:06	04:37	01:35	03:19	05:33	04:08

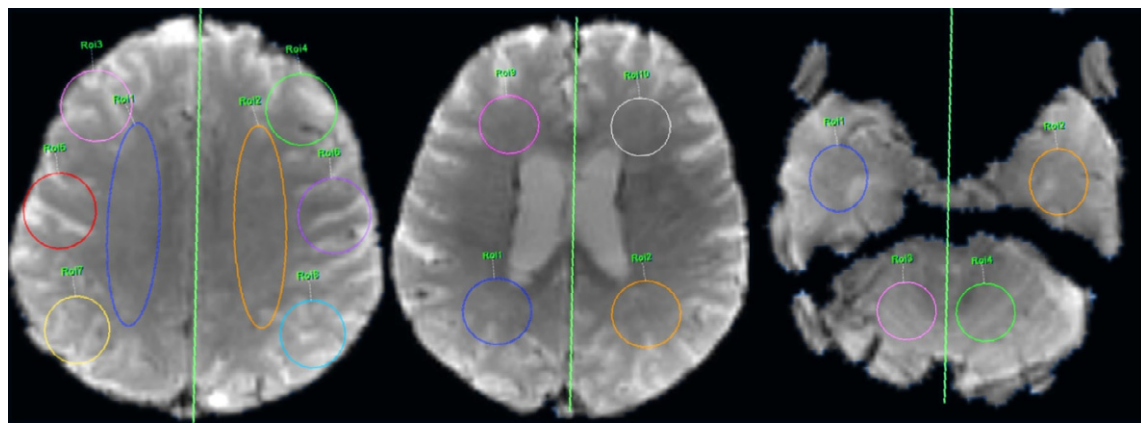


**Figure E1.** Placement of regions of interest for the brain MRI perfusion analysis  
ROI = region of interest. Green line representing the midline.

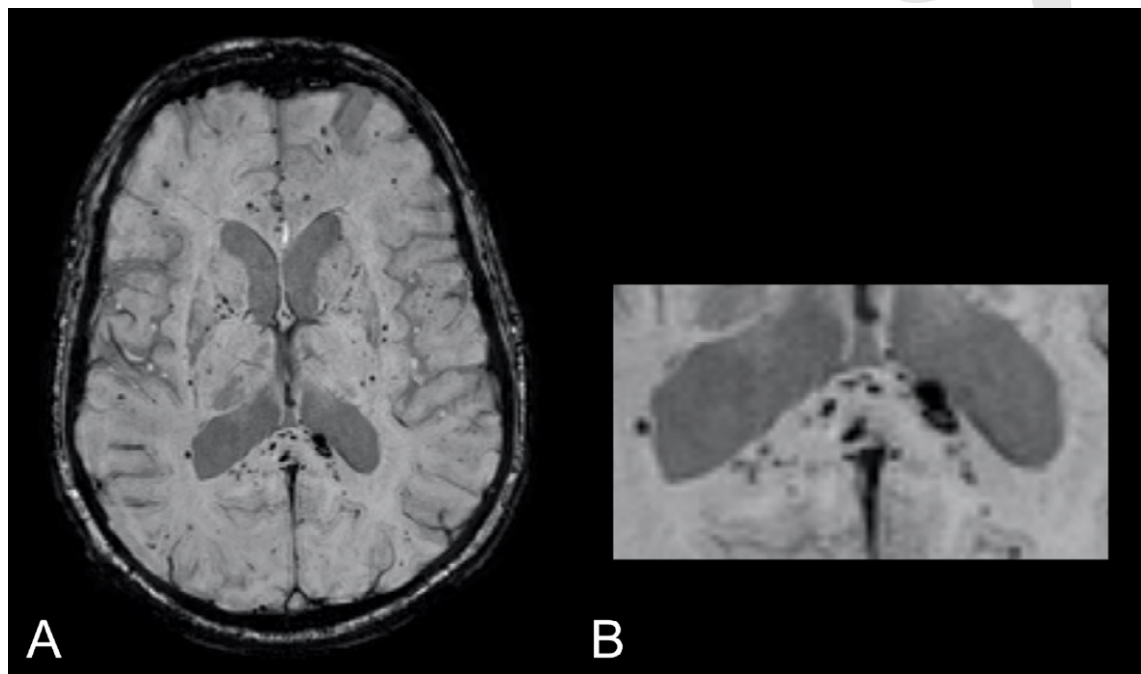


**Figure E2.** Non-spherical shape of SWI abnormalities.

Same patient as in Figure 2 A-D. Brain MRI with SWI in the axial view showing multiple susceptibility abnormalities (A) with predilection for the splenium of the corpus callosum (zoomed in, B) exhibiting an ovoid shape, suggestive of microvascular pathology along vessels or possibly the microstructure. SWI = susceptibility-weighted imaging.

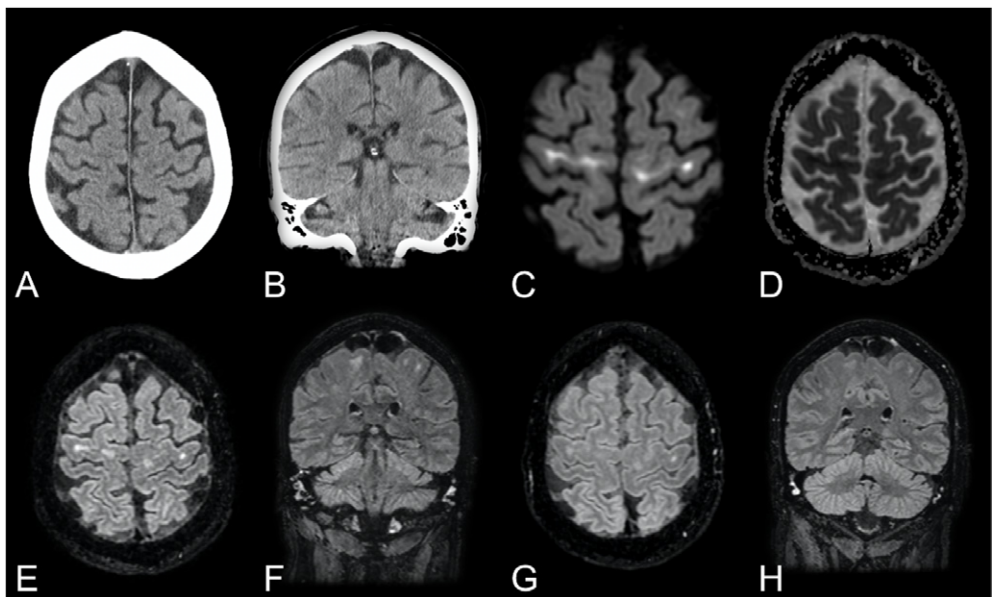


**Figure E3.** Longitudinal changes in white matter signal abnormalities.

Woman in her early 60s with COVID-19, multiorgan failure, sepsis and impaired consciousness (GCS 3) after 2 weeks in the ICU. Non-enhanced brain CT in the axial (A) and coronal (B) views reported as normal. Brain MRI with DWI b1000 (C) and ADC map (D) revealed reduced diffusion bilaterally in the precentral gyri. T<sub>2</sub>-weighted FLAIR images in the axial (E) and coronal (F) views demonstrated minor bilateral white matter changes in the same areas, possibly representing posterior reversible encephalopathy syndrome, although differential diagnoses included hypoxic changes and encephalitis. No susceptibility abnormalities were detected (image not shown). At MRI follow-up 5 days later, FLAIR changes had partially regressed (G-H), though the consciousness level of the patient remained unchanged. ADC = apparent diffusion coefficient, ARDS = Adult Respiratory Distress Syndrome, DWI = diffusion weighted imaging, FLAIR = fluid-attenuated inversion recovery, GCS = Glasgow coma scale, ICU = intensive care unit, SWI = susceptibility-weighted imaging.

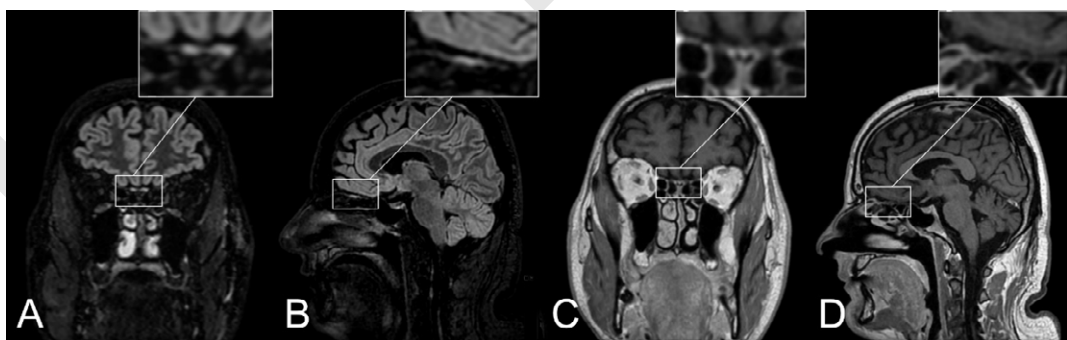
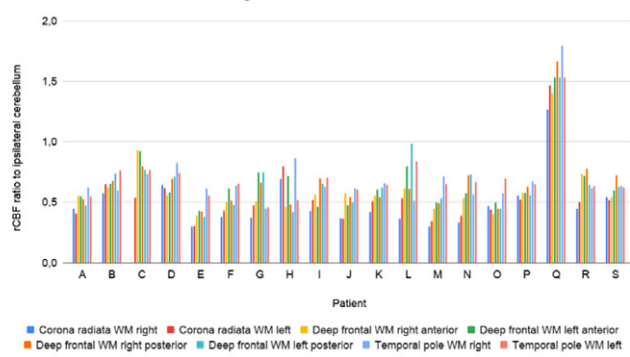


**Figure E4.** Olfactory bulb signal abnormalities.

Man in his early 40s with COVID-19. The patient had impaired cognition at the time of imaging and no history on olfactory symptoms was available. Brain MRI with non-enhanced T<sub>2</sub>-weighted FLAIR images in the coronal (A) and sagittal (B) views showing olfactory bulbs and tracts with higher signal intensity compared to the adjacent cortical gray matter. T<sub>1</sub>-weighted images post-contrast in the coronal (C) and sagittal (D) views exhibited subtle enhancement of the olfactory bulbs and tracts.

rCBF in white matter brain regions



rCBF in grey matter brain regions

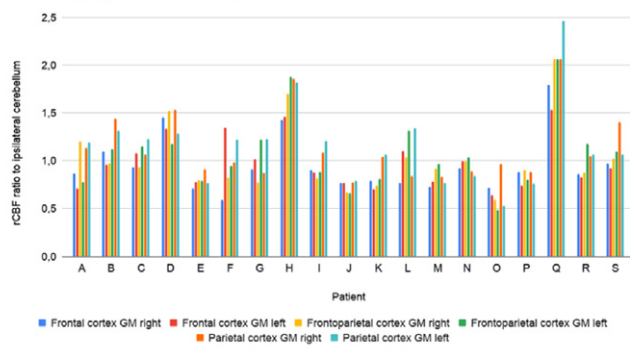


**Figure E5.** Brain dynamic susceptibility contrast MR perfusion results. GM = grey matter, rCBF = relative cerebral blood flow, WM = white matter. Letters A-S represents the 19 individual patients with perfusion MRI data. The relative cerebral blood flow was normalized against relative cerebellar blood flow to yield a rCBF ratio.